Dynamics of Atmospheres and Oceans 77 (2017) 89–99

Contents lists available at ScienceDirect

Dynamics of Atmospheres and Oceans

journal homepage: www.elsevier.com/locate/dynatmoce

Exploring the vertical extent of breaking internal wave turbulence above deep-sea topography

Hans van Haren

Royal Netherlands Institute for Sea Research (NIOZ), P.O. Box 59, 1790 AB Den Burg, the Netherlands

ARTICLE INFO

Article history:
Received 11 May 2016
Received in revised form 4 January 2017
Accepted 4 January 2017
Available online 7 January 2017

Keywords:
Internal wave turbulence
Sloping ocean topography
Wave breaking
400 m high mooring line
200 High-resolution temperature sensors

ABSTRACT

A mooring equipped with 200 high-resolution temperature sensors between 6 and 404 m above the bottom was moored in 1890 m water depth above a steep, about 10° slope of Mount Josephine, NE-Atlantic. The sensors have a precision of less than 0.5 mK. They are synchronized via induction every 4 h so that the 400 m range is measured to within 0.02 s, every 1 s. Thin cables and elliptical buoyancy assured vertical mooring motions to be smaller than 0.1 m under maximum 0.2 m s^{-1} current speeds. The local bottom slope is supercritical for semidiurnal internal tides by a factor of two. Exploring a one-month record in detail, the observations show: 1/semidiurnal tidal dominance in variations of dissipation rate ε, eddy diffusivity K_z and temperature, but no significant correlation between the records of ε and total kinetic energy, 2/a variation with time over four orders of magnitude of 100-m vertically averaged ε, 3/a local minimum in density stratification between 50 and 100 m above the bottom, 4/a gradual decrease in daily or longer averaged ε and K_z by one order of magnitude over a vertical distance of 250 m, upwards from 150 m above the bottom, 5/monthly mean values of $<[\varepsilon]> = 2 \pm 0.5 \times 10^{-7}$ m^2 s^{-3}, $<[K_z]> = 8 \pm 3 \times 10^{-3}$ m^2 s^{-1} averaged over the lower 150 m above the bottom.

1. Introduction

The impact of mechanical turbulent mixing in the ocean is considerable: without it there will be no life, no redistribution of nutrients and matter, and, typical for the deep-sea, no stable stratification in density as it also governs the downward transport of heat (Munk, 1966). Since Munk's suggestion, with follow-ups by Armi (1978, 1979), that most ocean mixing occurs in the vicinity of sloping bottom topography, efforts have been made to establish the dominant processes until to date, see for example a recent overview by Sarkar and Scotti (2017) focusing on modelling of internal waves generated by barotropic flow over topography.

Turbulent frictional effects by steady flows are quite different over topography compared to flat bottoms, (e.g., Weatherly and Martin, 1978; MacCready and Rhines, 1991). Topography is also a primary source and sink of internal waves supported by the stable density stratification (LeBlond and Mysak, 1978). In particular the breaking of internal waves that have amplitudes O(10–100) m, (e.g., van Haren, 2005; Levine and Boyd, 2006), may dominate turbulent mixing in the lower 100 m above the bottom to such extent that it is sufficient to maintain the entire ocean stratified, without the need of further mixing in the interior. This only holds if near-boundary mixing is efficient (Garrett, 1990), with the necessity to transport the homogeneous waters into the interior and replace them by stratified waters.

E-mail address: hans.van.haren@nioz.nl

http://dx.doi.org/10.1016/j.dynatmoce.2017.01.002
0377-0265/

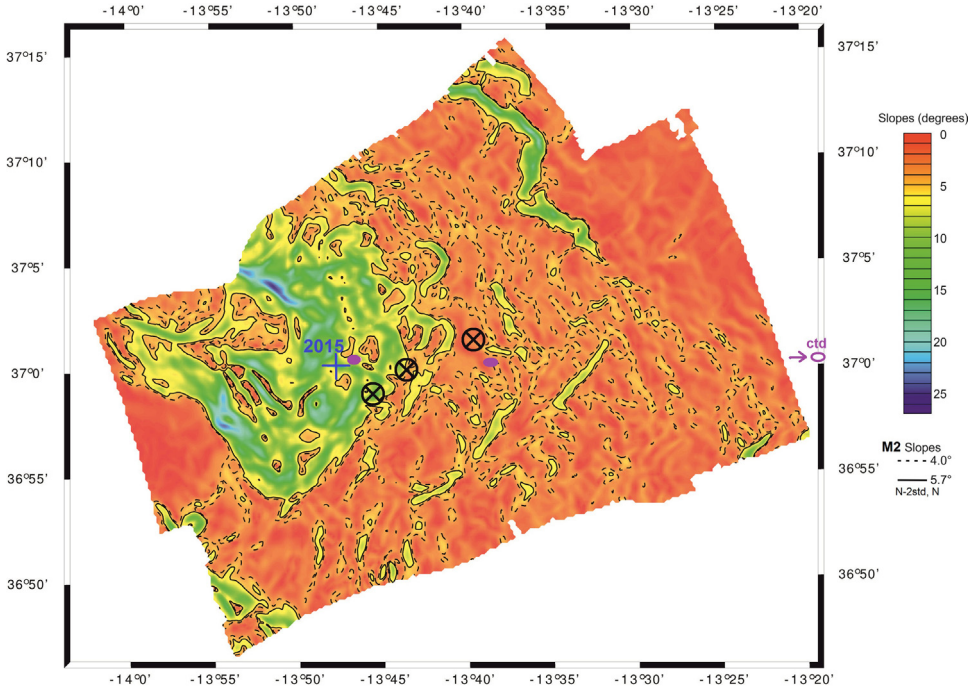

Fig. 1. Mooring area to the East of the southern sub-summit (37°02′N; 13°58′W) of Mount Josephine. The present site (blue) is shallower than three previous ones (black circle crosses) deployed in 2012–2013. Nearby and far CTD stations are indications by purple ellipses, one outside the page. Critical M_2 internal tidal slopes are computed for mean (N) and weak stratification (N-2 standard deviations). (For interpretation of the references to color in this figure legend, the reader is referred to the web version of this article.)

Detailed ocean temperature observations have demonstrated near-boundary turbulence in the deep-sea above sloping topography (Thorpe, 1987; van Haren et al., 1994). The latter experiment included microstructure profiler data down to 0.15 m from the bottom. Long-term mooring experiments above the Hawaiian Ridge, project 'HOME', established estimates of turbulence parameters monitoring 10–200 m vertical scales in 1500 and 2500 m water depth starting about 10 m from the bottom (Levine and Boyd, 2006; Aucan et al., 2006). These authors used SeaBird temperature sensors with an accuracy of several mK sampling at rates of 2–3 min in areas where the temperature-density relationship was sufficiently tight. In such areas temperature is an appropriate tracer for density so that the method of reordering vertical density profiles into stable ones can be used, as proposed by Thorpe (1977). During HOME, mean turbulence dissipation rate ε of 10^{-8} m^2 s^{-3} and vertical eddy diffusivity K_z of 10^{-3} m^2 s^{-1} were estimated for the lower 100 m near the bottom. Higher up, more than 100 m above the bottom, one tenth of these values were estimated.

Meanwhile and inspired by the instrumentation described in (Thorpe, 1987), the Royal Netherlands Institute for Sea Research NIOZ developed moorable high-resolution temperature sensors that were ten times more precise than SeaBird sensors (van Haren et al., 2001). As their power consumption was made very low, they could sample at a rate of 1 Hz, 100 times faster than the moored sensors in (Levine and Boyd, 2006; Aucan et al., 2006). Initially, such sampling rate could be maintained on one power supply for the duration of a month, later of a year (van Haren et al., 2009). This sensor set-up and the use of many, typically 100 sensors at 0.2–2 m vertical distances depending on the local stratification, became to reveal details of near-bottom internal wave-induced turbulence over sloping topography (van Haren, 2005; van Haren et al., 2015). Thus far over ranges of up to 100 m, such observations have shown high-frequency internal wave breaking is accompanied by the moving up and down of larger scale internal tidal waves that result in continual and rapid restratification to within a few meters from the bottom, (e.g., van Haren et al., 2015). In that study, moored data were compared from three different slope sites of Mount Josephine (black sites in Fig. 1), a large seamount in the NE-Atlantic Ocean. Most intense internal wave breaking was observed above slopes steeper, 'supercritical', than the slope of rays of the most energetic internal waves, at the semidiurnal lunar tidal M_2 frequency. The importance of steep bottom topography has recently been acknowledged in numerical modelling (Sarkar and Scotti, 2017). It contrasts with numerical simulations of internal wave breaking above concave and convex topography, showing intense turbulence at all slopes (Legg and Adcroft, 2003).

Over a distance of 100 m from the bottom, i.e. the intense mixing layer height over sloping topography suggested by (Armi, 1979; Garrett, 1990), considerable difference in turbulence temperature statistics was found between tidal phases and height above the bottom (Cimatoribus and van Haren, 2015). Turbulence was much stronger during the upslope tidal phase. In the lower 50 m, the temperature statistics were consistent with those of shear driven turbulence and inertial subrange. In the upper 50 m, the temperature statistics deviated from those of shear turbulence, and also evidence of turbulent convective activity was found.

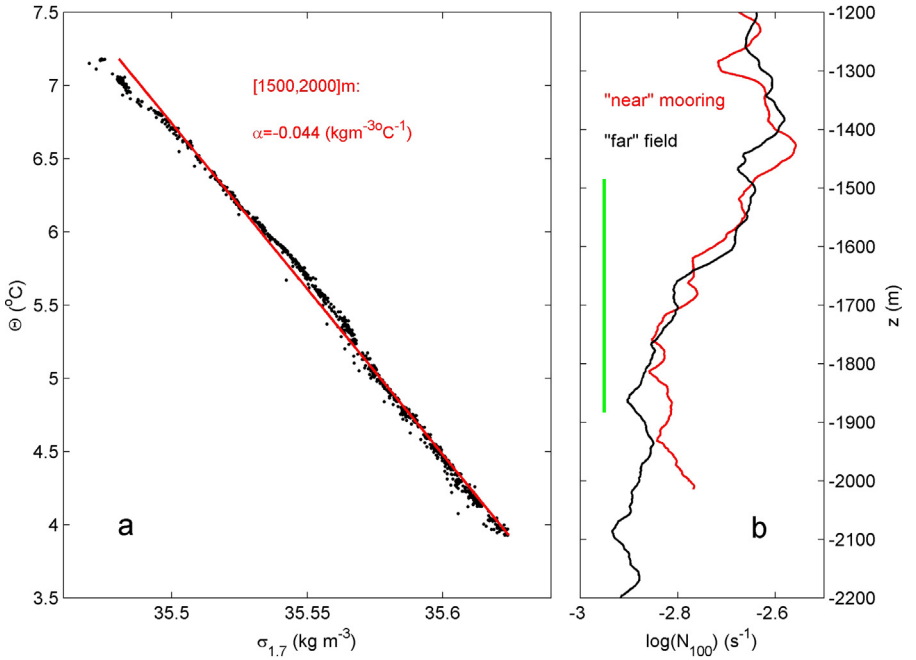

Fig. 2. Some CTD-observations. a. Conservative Temperature – density anomaly relationship established from nearby CTD observations for the range of moored temperature observations. b. Buoyancy frequency from stratification computed over 100 m vertical intervals from CTD near the mooring (red) and 80 km to the East (37°00′N; 12°58′W). (For interpretation of the references to color in this figure legend, the reader is referred to the web version of this article.)

In the present paper, the high-resolution ocean temperature observations are extended using 200 sensors over 400 m above the bottom to further explore the range of turbulence due to breaking internal waves above sloping topography. The observations will be compared with HOME observations (Levine and Boyd, 2006; Aucan et al., 2006) and with recent detailed 2D numerical model results (Winters, 2015) of an internal tide moving up and down a slope. This model uses a vertical scale height of the buoyancy length $\delta = U_0/\langle N \rangle$, where U_0 is a large velocity scale and <N> the large-scale buoyancy frequency determined over O (100 m) vertically. This vertical scale is dynamically important for turbulent motions. It is estimated 10 times larger than the Ozmidov scale in ocean observations (Cimatoribus and van Haren, 2015). Winters' model results give an isopycnal excursion height of $\eta \approx 1.25\delta$, a vertical extent of turbulence from the bottom in the breaker zone of $\Delta z = 4$–5δ and a lateral turbulence extent from the slope of $\Delta y = 15\delta$. The present observations are made from a fourth site above Mount Josephine (blue site in Fig. 1) where $U_0(M_2) = 0.1\ m\ s^{-1}$, $\langle N \rangle = 1.6 \times 10^{-3}\ s^{-1}$, so that $\delta \approx 60$ m. Following the numerical model by Winters (2015), we expect a vertical and horizontal extent of turbulence due to breaking waves of about 250 m and 900 m, respectively.

2. Technical details

As part of a seamount mooring program between 2012 and 2015, a 400 m long thermistor string array was located at 37°00′N, 013°47′W, 1890 m water depth on the eastern flank of Mount Josephine (Fig. 1), about 400 km southwest of Lisbon (Portugal) on 2 May 2015 (yearday 121). It was recovered in mid-August 2015. A total of 200 NIOZ4 high-resolution temperature 'T' sensors were taped to the nylon-coated 0.005 m diameter steel cable. A single large elliptic buoy was at 1463 m, 27 m above the uppermost T-sensor. The buoy provided 2200 N net buoyancy to the entire assembly. Under maximum 0.2 m s^{-1} current amplitudes, the low-drag mooring did not deflect from the vertical by more than 1°, i.e. the top-buoy moved <7 m horizontally and <0.1 m vertically. The average local bottom slope of about 10° is about twice supercritical than the average angle of semidiurnal internal tide rays under local stratification conditions (Fig. 1), (van Haren et al., 2015). The mooring was between 600 and 1000 m below the nearest sub-summit at 800 m water depth. Mount Josephine's absolute summit extends up to 250 m water depth. The mooring was also well below the Mediterranean Sea outflow, between 1000 and 1400 m, so that salinity compensated apparent density inversions in temperature are expected to be minimal.

The top-buoy held a 'down-looking' Teledyne/RDI 75 kHz, four beam acoustic Doppler current profiler (ADCP). It measures currents in three directions, **U** = [u, v, w], and echo intensity in each beam at 90 vertical bins of 5 m. The first bin was around the depth of the uppermost T-sensor. The lowest bin of good data was bin 70, at 1840 m, due to side-lobe reflection off the bottom. There, the beam spread or horizontal averaging distance for current components was about 250 m.

NIOZ4 are self-contained T-sensors sampling at 1 Hz, with a sensor tip smaller than 1 mm, a precision better than 5×10^{-4} °C after drift-correction and a noise level of $<1 \times 10^{-4}$ °C, see (van Haren et al., 2009) for the predecessor 'NIOZ3'

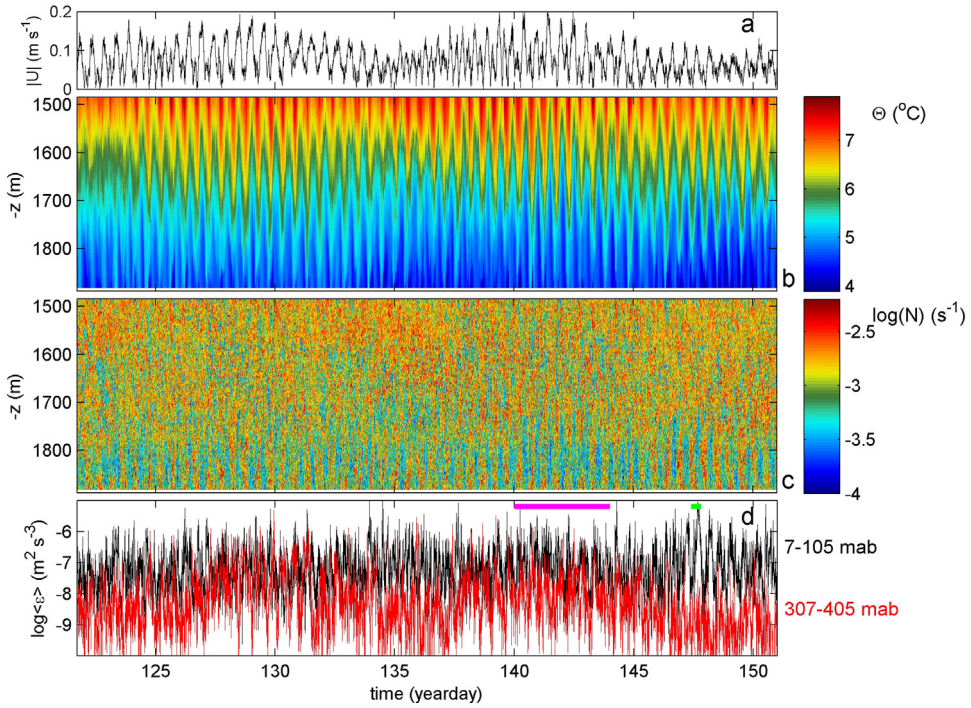

Fig. 3. One month (May 2015) of current, high-resolution temperature measurements and inferred turbulence parameter estimates. (a) Current amplitude, vertical average over entire ADCP-range of about [1850 1480] m. (b) Conservative Temperature. (c) Buoyancy frequency (log-scale) from vertically stably reordered data of panel-a. (d) Logarithm of mean dissipation rate, vertically averaged over ∼100 m for the ranges [1884 1782] m (black) and [1584 1482] m (red). The period of Fig. 5 is indicated by a purple bar, that of Fig. 10 by the green bar. (For interpretation of the references to color in this figure legend, the reader is referred to the web version of this article.)

with similar characteristics. Every four hours, all sensors are synchronized via induction to a single standard clock, so that the entire sensors range is sampled in less than 0.02 s. This, together with the relatively small mooring deflection, implies a near-instantaneous and near-vertical 'synoptic' view of temperature over a range of 400 m which is not achievable in standard moorings, via free-falling or lowered ship-borne instrumentation. An average advection speed of 0.1 m s^{-1} causes a horizontal mooring deflection of ±1 m half-way the T-sensor array compared to lowest and uppermost sensors, due to the 0.25° tilt. Such displacement is less than a factor of 10 smaller than, 1/the bottom slope and associated bottom-normal coordinates are in, say, the lower 30 m of frictional influence above the bottom (Weatherly and Martin, 1978; MacCready and Rhines, 1991), 2/sampling strategies are like shipborne Conductivity-Temperature-Depth 'CTD' or free-falling microstructure profiler 'MP'. The CTD and MP sampling takes 400–600 s to cross the range of moored T-sensors at standard vertical speeds by which structures measured at the depth of the uppermost T-sensor have been displaced horizontally by about 50 m compared with those measured at the lowest T-sensor, see (van Haren and Gostiaux, 2015) for examples.

The T-data are converted into 'Conservative' (∼potential) Temperature data Θ (IOC, SCOR, IAPSO, 2010). They are used as tracer for density anomaly σ variations following the relation $\delta\sigma_{1.7} = \alpha\delta\Theta$, $\alpha = -0.044 \pm 0.003$ kg m^{-3} °C^{-1} (Fig. 2a), where α denotes the apparent thermal expansion coefficient under local conditions and subscript 1.7 indicates 1700 m depth. This relation is established from data between 1500 and 2000 m of a shipborne CTD-profile within 1 km from the mooring site.

Thus, given the reasonably tight density-temperature relationship, the number of T-sensors and their spacing of 2.0 m, in combination with their low noise level, allows for accurately estimating turbulence parameters like dissipation rate ε and vertical eddy diffusivity K_z via the reordering of unstable overturns making every 1-Hz sampled 'density-'profile a statically stable one (Thorpe, 1977). As the present well-synchronized sensors are ten times more precise than in (Levine and Boyd, 2006; Aucan et al., 2006) and ten times more sensors are used over roughly the same range, thus resolving ten times smaller overturn scales, they are expected to refine the probably low-biased estimates in (Levine and Boyd, 2006; Aucan et al., 2006). This is verified here by sub-sampling the present data set by a factor of ten, which resulted in turbulence parameter estimates that were lower by factors of 0.25–0.95 depending on the period of wave breaking intensity, with a mean of a factor of 0.5. In addition, statistics are improved also because of the 100-times faster sampling rate and the 0.25 s response time of the sensors. Otherwise, identical methodology is used as proposed in (Thorpe, 1977) and used in, e.g., (Levine and Boyd, 2006; Aucan et al., 2006; Nash et al., 2007), see (van Haren and Gostiaux, 2012, 2015) for details. It includes a constant mixing efficiency of 0.2 (Osborn, 1980; Oakey, 1982), an Ozmidov L_O – rms overturn scale L_T ratio of $L_O/L_T = 0.8$ (Dillon, 1982) and

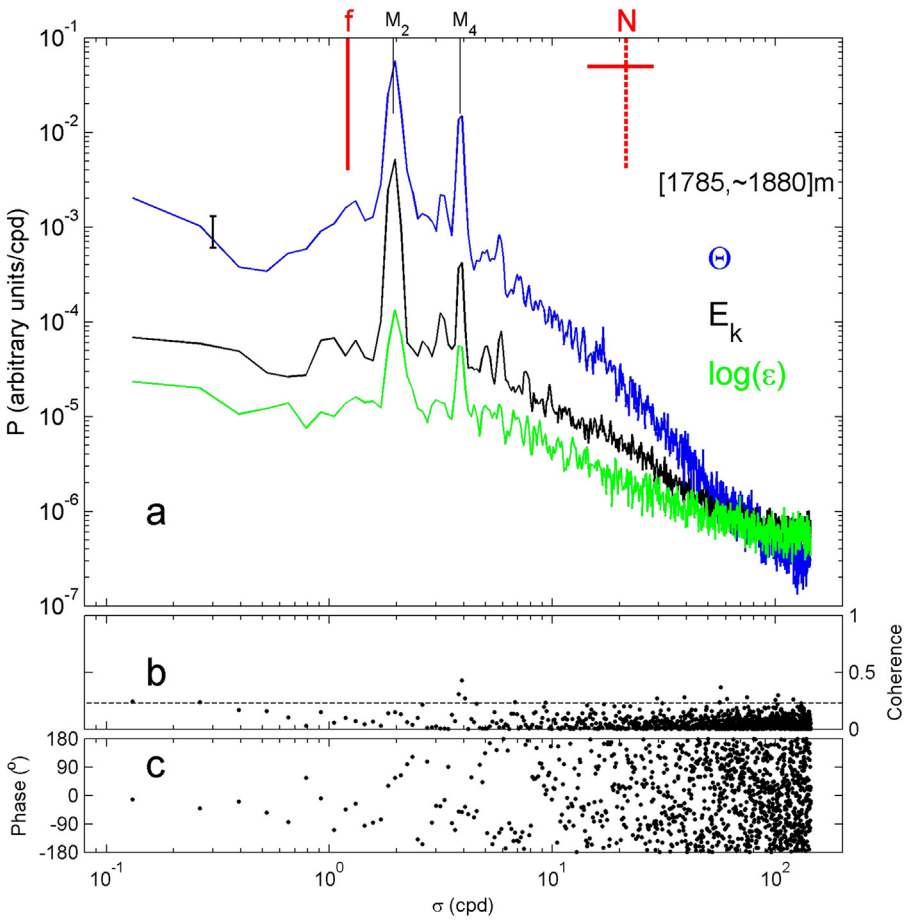

Fig. 4. Spectra from full length time series of vertically averaged data for the lower 100 m range of temperature sensors. a. Power spectra of temperature variance (blue), kinetic energy (black) and the logarithm of turbulence dissipation rate. b. Coherence between the logarithm of kinetic energy (to the power $1.5 \sim |U|^3$, representing KE-rate) and the logarithm of dissipation rate. The horizontal dashed line indicates the 95% significance level. c. Corresponding phase. (For interpretation of the references to color in this figure legend, the reader is referred to the web version of this article.)

the computation of buoyancy frequency N from the reordered stable density (temperature) profiles (Thorpe, 1977; Dillon, 1982). Thus, the familiar equations are used for turbulence parameter estimates,

$$\varepsilon = 0.64 L_T^2 N^3, \text{ the dissipation rate,}$$

$$K_z = 0.128 L_T^2 N, \text{ the eddy diffusivity.}$$

Recently, it has been shown that the mixing efficiency may vary with tidal cycle (Chalamalla and Sarkar, 2015) and that the ratio of turbulence scales is biased for convective turbulence (Mater et al., 2015). It will be demonstrated in the Appendix A that the average turbulence estimates from the present data using the above methodology are not affected to within one standard error, with respect to other observational methods like microstructure measurements.

In the following, averaging over time is denoted by [. . .], averaging over depth-range by <. . .>. The specific averaging periods and ranges are indicated with the mean values. In order to compute average buoyancy frequencies, stratification rates N^2 are averaged before the square root is taken. Mean eddy diffusivities are computed by averaging heat fluxes, before computing mean K_z.

3. Observations

Focusing on the first month of data (Fig. 3), semidiurnal tidal motions dominate currents (Fig. 3a) and temperature variations (Fig. 3b) over the entire 400 m range of observations. During springtide in currents, e.g. on days 128 and 142, the T-excursions exceed a vertical range of 200 m crest-trough, like in HOME (Levine and Boyd, 2006; Aucan et al., 2006). The isotherm excursions seem to vary regularly tidally, with warmer waters above cooler providing stable density stratification. However, in comparison with currents, their modulation is less clearly spring-neaps as excursion peaks are also observed at,

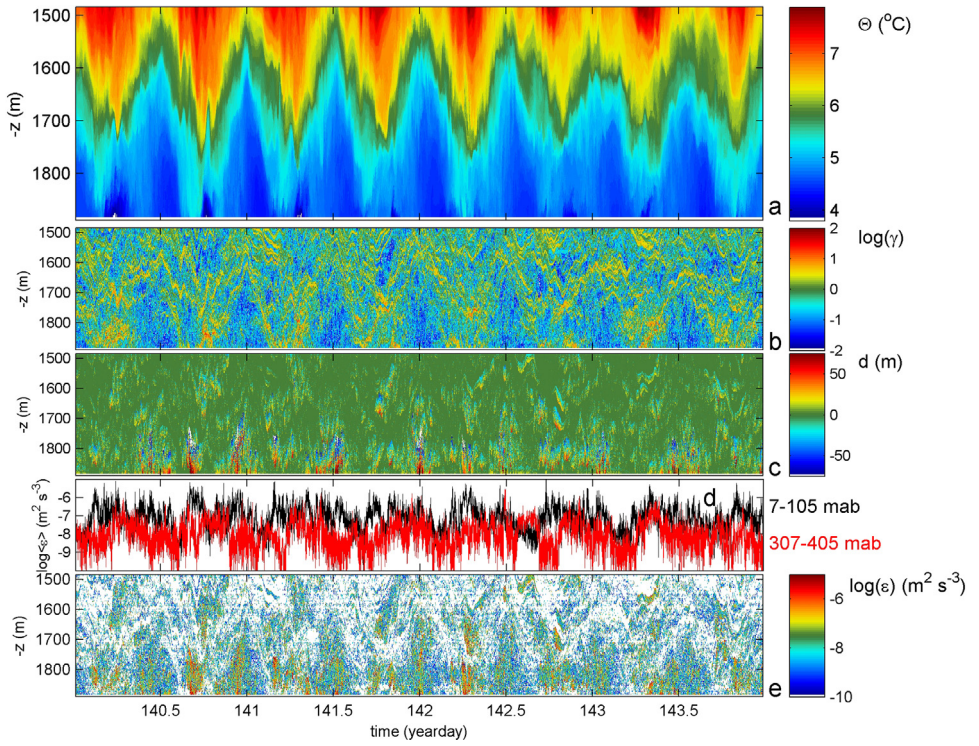

Fig. 5. Four-day detail of temperature and inferred turbulence measurements of purple bar in Fig. 3, with full time-depth panels on strain (b), displacements after reordering (c) and the logarithm of turbulence dissipation rate (e).

e.g., days 131 and 147. Furthermore, as will be shown below, the tidal motions do not represent linear internal waves, but highly nonlinear ones with regular turbulent overturning. This shows partially in the density stratification, represented by local N using reordered Θ and $\Delta z = 2$ m vertical length-scale (Fig. 3c). In this time-depth image, semidiurnal tidal variations weakly dominate in the lower 100–150 m above the bottom only. In that near-bottom range, a concentration of weak stratification is found at about 50–100 m above the bottom when waters are coolest. Higher-up, a regular tidal periodicity is unclear. N is found to vary from near-homogeneous, $N \sim 10^{-4}$ s^{-1}, to relatively strong, $N \sim 3 \times 10^{-3}$ s^{-1}, within a few hours, even very close to the bottom. Due to such short-term variations, also 100-m-averaged turbulence dissipation rate estimates show only weak semidiurnal tidal dominance of variation with time, foremost in the near-bottom 100 m (represented by $<\varepsilon>$ in Fig. 3d). A spring-neap cycle is not well visible in these data. In general, this vertically averaged turbulence dissipation rate is one order of magnitude smaller for the range between 300 and 400 m above the bottom (red in Fig. 3d) compared with estimates for the lower 100 m of the temperature sensor range (black in Fig. 3d). However, exceptions exist with larger turbulence values higher up over brief periods, e.g., on days 130 and 136.

Although the spectrum of $\log<\varepsilon>$ shows significant peaks at semi- and fourth-diurnal frequencies, such peaks in temperature and kinetic energy are considerably more pronounced (Fig. 4a). The coherence between large-scale kinetic energy rate $|U|^3$ and ε is not found significant at any frequency, while the one with $\log<\varepsilon>$ shows a single barely significant value at M_4 (Fig. 4b,c). This contrasts with the findings during HOME (Levine and Boyd, 2006), but is typical for previous seamount observations in the NE-Atlantic (van Haren et al., 2015; Cimatoribus and van Haren, 2015).

In a four day detail of the current-springtide period around day 142, the dominant semidiurnal variations are seen superposed with higher-frequency, smaller-scale motions (Fig. 5a). The tidally alternating strongly and weakly stratified waters in the lower 150 m above the bottom show large variations in strain $\gamma = \partial\eta/\partial z = N^2/[N^2]$, following (Sherman and Pinkel, 1991), with values reaching as low as 0.01 in weak stratification (Fig. 5b). In weaker stratified, low strain periods and ranges, like in the lower 150 m around day 142.0, unstable overturn displacements exceed the vertical range of $\pm$75 m (Fig. 5c). Large dissipation rates associated with $\sim$50 m overturns are also found around fronts, e.g., on day 142.2. In general, this 100–150 m range above the bottom contains most of the higher turbulence dissipation rate values (Fig. 5d). Instantaneous high values, which should at least be integrated over the size of the respective overturn following (Thorpe, 1977), group in a more or less fourth-diurnal tidal-harmonic variation pattern for the near-bottom range over this period (Fig. 5e).

The above depth-time observations are summarized after averaging the turbulence and stratification estimates over time, for periods varying from a month to three hours (Fig. 6). Both mean turbulence dissipation rate (from 2×10^{-7} to 2×10^{-8} m^2 s^{-3}; Fig. 6a) and eddy diffusivity (from 3×10^{-2} to 2×10^{-3} m^2 s^{-1}; Fig. 6b) decrease by a factor of about 10, one order of magnitude, over the 400 m range. Similar one order of magnitude decrease over about 200 m was observed above the Hawaiian Ridge (Levine and Boyd, 2006). There however, values were estimated one order of magnitude lower than the

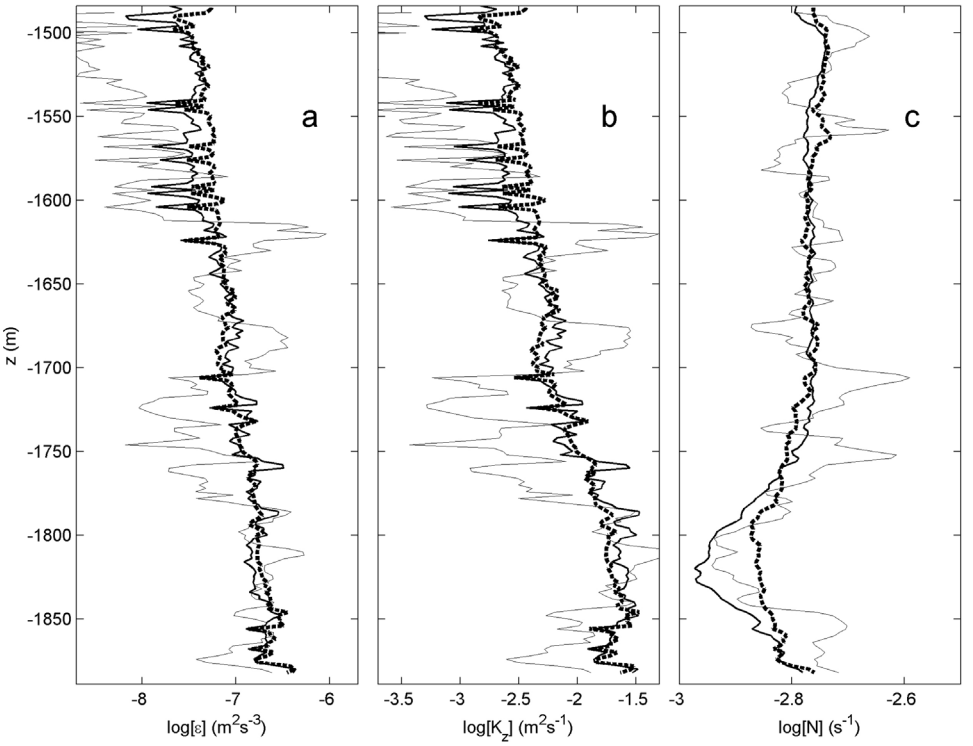

Fig. 6. Full depth profiles of logarithms of time-averaged parameter values (the local water depth is at 1890 m, the level of the x-axes). One month (Fig. 3) averages are indicated by thick-dashed lines, four day averages (Fig. 5) by thick-solid lines and three hour (Fig. 8) averages by thin-solid lines. (a) Turbulence dissipation rate. (b) Vertical turbulence diffusivity. (c) Buoyancy frequency with x-axis having the same range as in Fig. 2b.

present ones. Here, mean stratification remains about the same very close to the bottom, noting that the lowest sensor was still 6 m above the bottom, and most of the range higher-up (Fig. 6c), with values close to those observed by CTD (Fig. 2b). The featureless [N](z) explains the highly similar time-depth images of strain and stratification. A small exception to a vertically constant [N] is the vertical range between 40 and 120 m above the bottom, across which stratification shows a significant minimum that is most pronounced during spring tide. Below this layer down to 6 m above the bottom, stratification increases and time-mean turbulence parameters weakly decrease from their maximum values at about 50–100 m above the bottom. Apparently, the heat flux becomes negligible only in a very thin layer above the bottom, below the present lowest T-sensor. This confirms previous observations using T-sensors down between 0.5 and 50 m from the bottom at 0.5 m intervals (van Haren and Gostiaux, 2012) and microstructure data down to 0.15 m from a sloping bottom (van Haren et al., 1994).

In Fig. 6, scatter is large in short-period averages (thin lines in Fig. 6 as an example). Except for the near-bottom increase, [N](z) is similar to the far-field stratification from CTD (black curve in Fig. 2b). Smoothed profiles of 4 and 31 days averages show relatively little difference, except for the stratification minimum, with a layer of high turbulence parameter values extending from the near-bottom up to z = −1760 m. The jump to lower values at about z = −1700 m is more pronounced in diffusivity than in dissipation rate. Above this depth, stratification weakly increases with height above the bottom at relatively high values.

The transition from lower to higher dissipation rate values is still visible in further detailed time-depth images, like the one day zoom of Fig. 7. Large dissipation rates are not only associated with near-homogeneous waters, but also occur on the edges of relatively strong stratification. Interior wave breaking is seldom more turbulent than in the lower 100 m near the bottom. This suggests that wave breaking is not an independent process over the 400 m range, but a coupled process under the assumption of most intense breaking near the bottom, even over such a large vertical range of several 100's of meters. Obviously, this must then be related with the dominant, tidal, carrier wave, as the wave's moving back and forth over the sloping topography with a 100–200 m amplitude is the only process that is of the same order of magnitude as the 400 m range of observations.

The turbulent overturning associated with internal wave breaking is also reflected in the multiple layering of the density stratification. Zooming-in further to a 3-h period (Fig. 8) shows a gradually smoother lining-up of thin layers higher-up. There nevertheless, up to 100 m high near-homogeneous layers occur, e.g., between 1600 and 1700 m, lasting up to 1 h which is close to the local mean buoyancy period of 4000 ± 500 s. The seemingly weak turbulence dissipation rate still has a mean value $O(10^{-8})$ m^2 s^{-3} throughout.

A detail example of this turbulence affecting the T-field in the interior is shown in Fig. 9. Considering the ruggedness of the now more detailed isotherm-contour lines may have one appreciate the ε-value of 10^{-8} m^2 s^{-3}. Here, the form of turbulent

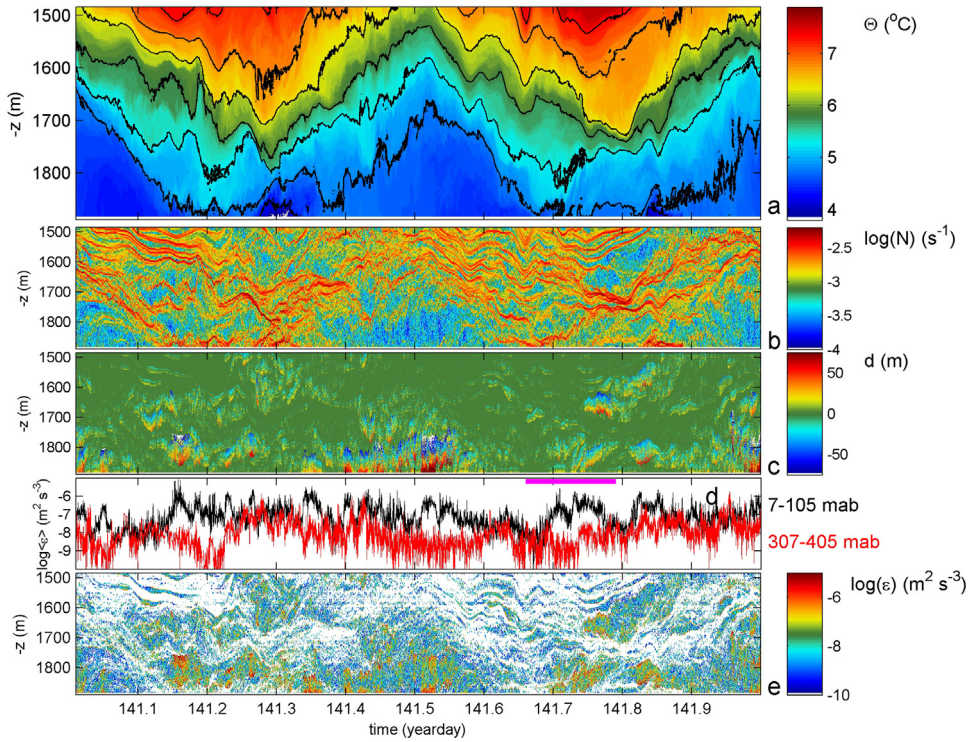

Fig. 7. As Fig. 5, but for one day (May 22). The black contours in panel-a are drawn every 0.5 °C. The purple bar indicates the period of Fig. 8. (For interpretation of the references to color in this figure legend, the reader is referred to the web version of this article.)

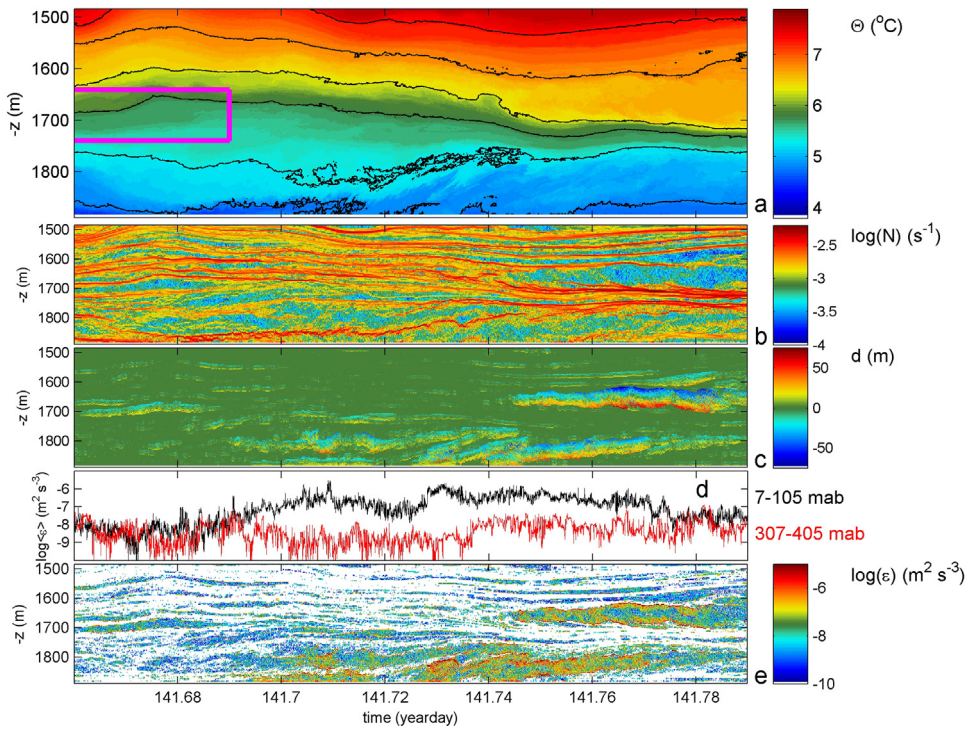

Fig. 8. Three-hour example detail of Fig. 7. The purple rectangle in panel a. indicates the time-depth period of Fig. 9. (For interpretation of the references to color in this figure legend, the reader is referred to the web version of this article.)

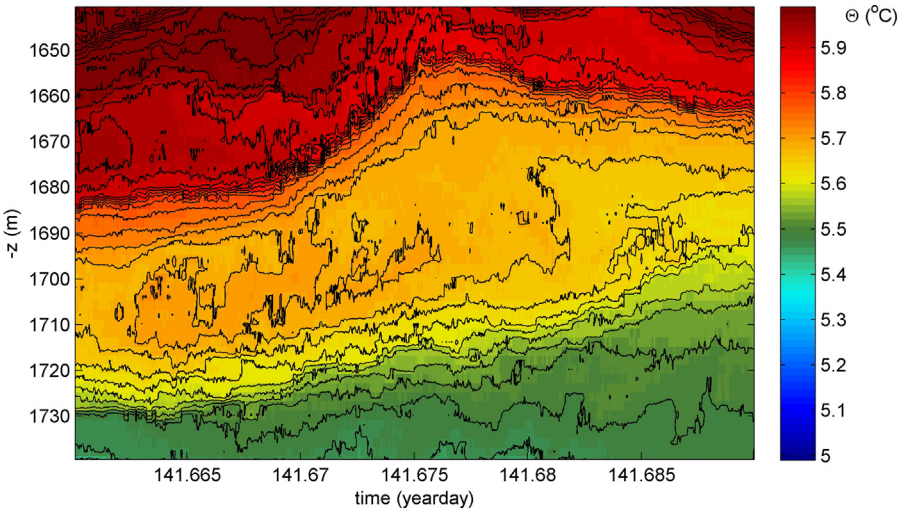

Fig. 9. Detail of Fig. 8a, with different colour-range contours every 0.025 °C. (For interpretation of the references to color in this figure legend, the reader is referred to the web version of this article.)

overturning does not represent classic examples of organized structure like Kelvin-Helmholtz or Holmboe instability. The overturns form single loops with smaller-scale instability that causes the rugged isotherms, in a fashion that is best described as free convective overturning initiated by shear, see for example modelling results by (Matsumoto and Hoshino, 2004).

A detailed example of an anomalously large near-bottom turbulent overturning is given in Fig. 10. This larger than 100 m overturning in near-homogeneous waters, where $[<N>] = 8 \times 10^{-4}\,s^{-1}$ in the near-bottom 100 m between days 147.63 and 147.76, lasts about 8000 s, commensurate the mean buoyancy period.

4. Discussion

The vertical range of 100–150 m above the bottom exhibiting consistently high levels of estimated turbulence is foremost generated by the breaking of internal waves and less by bottom friction. This confirms previous estimates made using the same methodology but coarser resolving instrumentation from the Hawaiian Ridge (Levine and Boyd, 2006; Aucan et al., 2006), although the present ones show values an order of magnitude larger. It also confirms high-resolution numerical modeling (Winters, 2015) of turbulence generation via internal wave sloshing and breaking over a slope. Similar with those model results, the present observations demonstrate such turbulence extending at least 300 m above the bottom. However, even between 300 and 400 m above the bottom turbulence parameter values still exceed those found in the open ocean interior, e.g., in (Gregg, 1989), by more than one order of magnitude. From the present observations we note that the rate and scale of turbulence overturning changes upward from about 150 m above the bottom. Both scales are higher than the, remarkably well-chosen, vertical scale height of 100 m of intense mixing over sloping topography considered by (Armi, 1979; Garrett, 1990) sufficient to maintain the ocean vertically stratified in density. The present high-resolution T-observations, like previous ones that approached the bottom to within 1 m from different areas, e.g., (van Haren et al., 2009; van Haren and Gostiaux, 2012), demonstrate that the near-bottom range above sloping topography is rapidly restratified. The mixing of different density layers in this high Reynolds number flow regime is thus expected to be efficient.

The picture that emerges is as follows. Most intense wave breaking is observed to occur at slopes steeper than those of the semidiurnal internal tide rays. Instead of critical principal tide reflection, which is not found relevant here, it is speculated that either a nonlinear energy transfer to phase-locked higher harmonics occurs or a freely propagating internal wave frequency higher than that of the back and forth moving tide can be found of which the rays critically match that of the slope. The latter assumes that the slope is subcritical for waves near <N>. For the present observations the average critical slope is for fourth-diurnal internal wave frequencies, approximately. After the breaking of the highly nonlinear motions, the larger-scale tide and sub-inertial motions transport mixed waters into the interior and restratify the near-bottom boundary. As the ocean-interior turbulence levels are not observed in the present 400-m range over the 10°-slope except for brief intervals, the horizontal extent of high turbulence levels exceeding open-ocean values by a factor of more than 10 is expected to reach at least 2000 m horizontally from the mount. This distance is twice the numerical model-result by Winters (2015).

Extrapolating these results to global ocean topography and considering the area of high turbulence levels in comparison with presumed low turbulence over 'flat, small' topography, as proposed by (Armi, 1979; Garrett, 1990), indicates more than sufficient turbulence generation by internal wave breaking to maintain the ocean stratification. Also, sufficient turbulence is expected to resuspend materials necessary for deep-sea life.

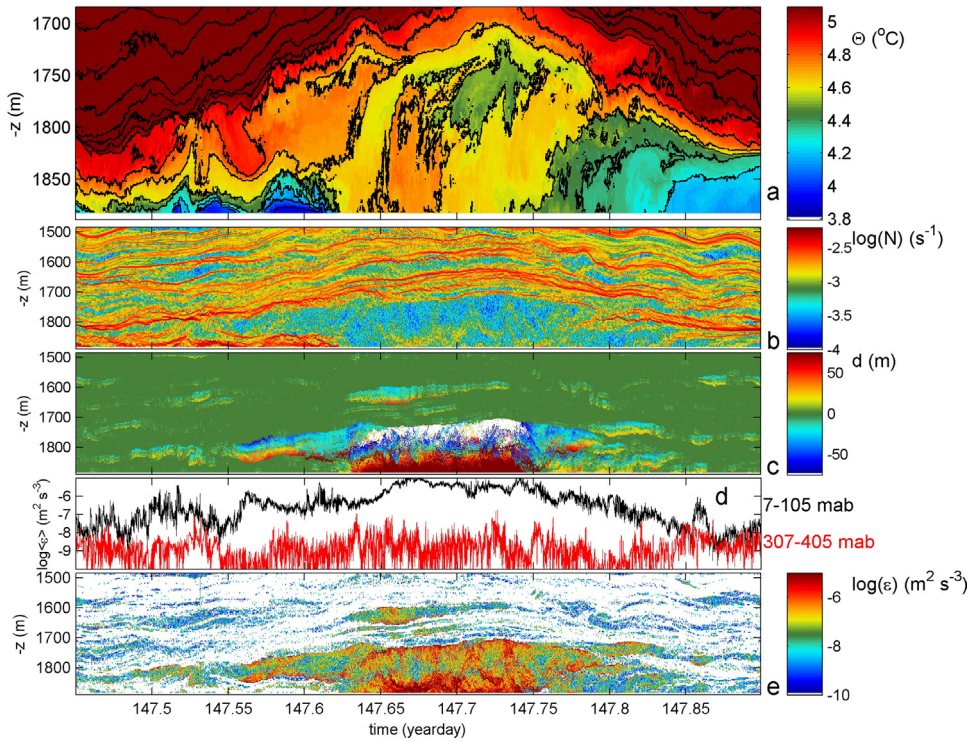

Fig. 10. Detail of Fig. 3 (green bar), with different colour-range contours every 0.15 °C. Panel a. is clipped in the vertical and in colour range, showing details of the lower 200 m. (For interpretation of the references to color in this figure legend, the reader is referred to the web version of this article.)

Acknowledgements

I thank the captain and crew of the R/V Pelagia and NIOZ-MTM for their very helpful assistance during deployment and recovery. Special thermistor thanks to M. Laan, A. Cimatoribus, F. van Maarsseveen.

Appendix A.

Recently, some concerns are raised that the mixing efficiency is not constant, with a value of 0.2, but may vary with tidal cycle (Chalamalla and Sarkar, 2015) and that the ratio of turbulence scales can be biased high for convective turbulence so that Thorpe overturning scales are larger than the Ozmidov scale, $L_T > L_O$ (Mater et al., 2015). Although such concerns are appreciated as they give insight in specific ocean turbulence processes of which knowledge is still lacking, their impact is modest. Modeling results (Chalamalla and Sarkar, 2015) show a range of variations in mixing efficiency between about 0.05–0.1 and 0.6–0.7 over a tidal cycle, while the mean was found very close to Osborn's (1980) mean value of 0.2. This one order of magnitude of variations was also reported for ocean observations by Oakey (1982). Likewise, Mater et al. (2015) show a factor of 3 increase in L_T over L_O can occur in convective turbulence, resulting in a one order of magnitude increase in dissipation rate. Such an increase is not observed for shear-induced turbulence, and, in fact, Mater et al. (2015) report a slightly larger mean value of about 1 than the canonical mean of 0.8 for their L_O/L_T ratio for averages over a certain time and depth of ocean observations. Such averaging was originally proposed by Thorpe (1977). The observations presented here and, e.g., from microstructure profiler data (Gregg, 1989), vary over at least four orders of magnitude as is common for ocean turbulence. This range of variations is much larger than any bias reported by Mater et al. (2015).

There are several reasons why the above recent concerns are unlikely to affect the turbulence parameter estimates computed from the present high-resolution moored T-sensor data using the familiar parameterizations given in Section 2.

First, although the estimates are made for every single 1-Hz profile and sensor depth, estimates are evaluated that are averaged over suitable length and time scales, of, say, 100 m in the vertical and the buoyancy scale, a tidal cycle or longer, respectively.

Second, the present observations are made from above steep topography where internal wave breaking and rapid restratification occur. In such dynamic environment, shear-induced turbulence and convective turbulence alternate, but shear-induced turbulence dominates and an inertial subrange has been observed (Cimatoribus and van Haren, 2015). In an environment where shear-induced turbulence dominates and an inertial subrange exists, the Ozmidov and Thorpe overturn scales are near-equal (Mater et al., 2015). This is expected as the internal wave field in such environment may cause highly intermittent turbulence, but a delicate balance between shear and stratification leads to marginal stability of quasi-

permanent nature. This is because the dominant shear-production comes from circular motions on a rotating sphere near the inertial and tidal frequencies (van Haren et al., 1999).

Third, as in any turbulence development, shear- and convective-turbulence intermingle and are hard to separate. Examples of numerical modelling studies of particular stages of instability developments show that a finger of convective instability develops secondary shear instability along its fringe (Li and Li, 2006), while the roll-up stage of shear instability develops secondary convective instability mushrooms (Matsumoto and Hoshino, 2004).

Fourth, comparison between turbulence estimates using shear measurements and using Thorpe overturning scales from areas with such mixtures of turbulence development above sloping ocean topography led to 'consistent results' (Nash et al., 2007) and 'results similar to within a factor of three' (van Haren and Gostiaux, 2012). A factor of two is the minimum error range for turbulence parameter estimates (Oakey, 1982).

Thus, from the argumentation above and the reasoning in Mater et al. (2015), internal wave breaking above sloping topography unlikely biases turbulence dissipation rates computed from Thorpe overturning scales by more than a factor of two-three, provided some suitable averaging is done instead of considering single profiles.

References

Armi, L., 1978. Some evidence for boundary mixing in the deep ocean. J. Geophys. Res. 83, 1971–1979.
Armi, L., 1979. Effects of variations in eddy diffusivity on property distributions in the oceans. J. Mar. Res. 37, 515–530.
Aucan, J., Merrifield, M.A., Luther, D.S., Flament, P., 2006. Tidal mixing events on the deep flanks of Kaena Ridge, Hawaii. J. Phys. Oceanogr. 36, 1202–1219.
Chalamalla, V.K., Sarkar, S., 2015. Mixing, dissipation rate, and their overturn-based estimates in a near-bottom turbulent flow driven by internal tides. J. Phys. Oceanogr. 45, 1969–1983.
Cimatoribus, A.A., van Haren, H., 2015. Temperature statistics above a deep-ocean sloping boundary. J. Fluid Mech. 775, 415–435.
Dillon, T.M., 1982. Vertical overturns: a comparison of Thorpe and Ozmidov length scales. J. Geophys. Res. 87, 9601–9613.
Garrett, C., 1990. The role of secondary circulation in boundary mixing. J. Geophys. Res. 95, 989–993.
Gregg, M.C., 1989. Scaling turbulent dissipation in the thermocline. J. Geophys. Res. 94, 9686–9698.
IOC, SCOR, IAPSO, 2010. The International Thermodynamic Equation of Seawater-2010: Calculation and Use of Thermodynamic Properties. Intergovernmental Oceanographic Commission, Manuals and Guides No. 56. UNESCO, Paris, France, 196 pp.
LeBlond, P.H., Mysak, L.A., 1978. Waves in the Ocean. Elsevier, New York, pp. 602.
Legg, S., Adcroft, A., 2003. Internal wave breaking at concave and convex continental slopes. J. Phys. Oceanogr. 33, 2224–2246.
Levine, M., Boyd, T.J., 2006. Tidally forced internal waves and overturns observed on slope: results from HOME. J. Phys. Oceanogr. 36, 1184–1201.
Li, S., Li, H., 2006. Parallel AMR code for compressible MHD and HD equations. T-7, MS B284, Theoretical division, Los Alamos National Laboratory, http://math.lanl.gov/Research/Highlights/amrmhd.shtml.
MacCready, P., Rhines, P.B., 1991. Buoyant inhibition of Ekman transport on a slope and its effect on stratified spin-up. J. Fluid Mech. 223, 631–651.
Mater, B.D., Venayagamoorthy, S.K., St Laurent, L., Moum, J.N., 2015. Biases in Thorpe scale estimates of turbulence dissipation. Part I: assessments from large-scale overturns in oceanographic data. J. Phys. Oceanogr. 45, 2497–2521.
Matsumoto, Y., Hoshino, M., 2004. Onset of turbulence by a Kelvin-Helmholtz vortex. Geophys. Res. Lett. 31, L02807, http://dx.doi.org/10.1029/2003GL018195.
Munk, W., 1966. Abyssal recipes. Deep-Sea Res. 13, 707–730.
Nash, J.D., Alford, M.H., Kunze, E., Martini, K., Kelly, S., 2007. Hotspots of deep ocean mixing on the Oregon. Geophys. Res. Lett. 34, L01605, http://dx.doi.org/10.1029/2006GL028170.
Oakey, N.S., 1982. Determination of the rate of dissipation of turbulent energy from simultaneous temperature and velocity shear microstructure measurements. J. Phys. Oceanogr. 12, 256–271.
Osborn, T.R., 1980. Estimates of the local rate of vertical diffusion from dissipation measurements. J. Phys. Oceanogr. 10, 83–89.
Sarkar, S., Scotti, A., 2017. From topographic internal gravity waves to turbulence. Ann. Rev. Fluid Mech. 49, 195–220.
Sherman, J.T., Pinkel, R., 1991. Estimates of the vertical wavenumber-frequency spectra of vertical shear and strain. J. Phys. Oceanogr. 21, 292–303.
Thorpe, S.A., 1977. Turbulence and mixing in a Scottish loch. Philos. Trans. R. Soc. Lond. A 286, 125–181.
Thorpe, S.A., 1987. Transitional phenomena and the development of turbulence in stratified fluids: a review. J. Geophys. Res. 92, 5231–5248.
van Haren, H., 2005. Details of stratification in a sloping bottom boundary layer of Great Meteor Seamount. Geophys. Res. Lett. 32, L07606, http://dx.doi.org/10.1029/2004GL022298.
van Haren, H., Gostiaux, L., 2012. Detailed internal wave mixing observed above a deep-ocean slope. J. Mar. Res. 70, 173–197.
van Haren, H., Gostiaux, L., 2015. Distinguishing turbulent overturns in high-sampling-rate moored thermistor string observations. J. Mar. Res. 73, 17–32.
van Haren, H., Oakey, N., Garrett, C., 1994. Measurements of internal wave band eddy fluxes above a sloping bottom. J. Mar. Res. 52, 909–946.
van Haren, H., Maas, L., Zimmerman, J.T.F., Ridderinkhof, H., Malschaert, H., 1999. Strong inertial currents and marginal internal wave stability in the central North Sea. Geophys. Res. Lett. 26, 2993–2996.
van Haren, H., Groenewegen, R., Laan, M., Koster, B., 2001. A fast and accurate thermistor string. J. Atmos. Oceanic Technol. 18, 256–265.
van Haren, H., Laan, M., Buijsman, D.-J., Gostiaux, L., Smit, M.G., Keijzer, E., 2009. NIOZ3: independent temperature sensors sampling yearlong data at a rate of 1 Hz. IEEE J. Ocean. Eng. 34, 315–322.
van Haren, H., Cimatoribus, A., Gostiaux, L., 2015. Where large deep-ocean waves break. Geophys. Res. Lett. 42, 2351–2357, http://dx.doi.org/10.1002/2015GL063329.
Weatherly, G.L., Martin, P.J., 1978. On the structure and dynamics of the oceanic bottom boundary layer. J. Phys. Oceanogr. 8, 557–570.
Winters, K.B., 2015. Tidally driven mixing and dissipation in the boundary layer above steep submarine topography. Geophys. Res. Lett. 42, 7123–7130, http://dx.doi.org/10.1002/2015GL064676.